ChemComm

Translating Aqueous CO2 Hydrogenation Activity to Electrocatalytic Reduction with a Homogeneous Cobalt Catalyst

Journal:	*ChemComm*
Manuscript ID	CC-COM-10-2022-005473.R2
Article Type:	Communication

COMMUNICATION

Translating Aqueous CO_2 Hydrogenation Activity to Electrocatalytic Reduction with a Homogeneous Cobalt Catalyst

Xinran S. Wang, Jenny Y. Yang*

Received 00th January 20xx,
Accepted 00th January 20xx

DOI: 10.1039/x0xx00000x

A molecular cobalt CO_2 hydrogenation catalyst was explored for electrocatalytic CO_2 reduction under aqueous conditions. The resulting pH-dependent selectivity between H_2 and HCO_2^- is rationalized with thermodynamic analysis and stoichiometric experiments.

The reduction of CO_2, either through hydrogenation or electrochemical pathways, is an attractive route to non-fossil carbon products,.[1–3] Hydrogenation catalysts typically generate a metal hydride intermediate from hydrogen and a base (**Scheme 1**, red). The parallel electrochemical 'hydrogenation' route uses two electrons from the electrode and a proton from solution to generate equivalent metal hydrides (**Scheme 1**, blue). An advantage of electrochemical reduction is that it directly uses electricity for CO_2 reduction instead of using H_2 as an intermediary reductant.

Extensive work has been performed on the development of both molecular CO_2 hydrogenation catalysts and electrocatalysts. However, there are few examples of translating reactivity between these two reduction mechanisms.[4,5] To further our understanding, we investigated the aqueous CO_2 hydrogenation catalyst $[Co(dmpe)_2(H)]^{2+}$ (**2**) (dmpe = 1,2-*bis*(dimethylphosphino)ethane) for electrocatalytic reduction. **2** exhibits one of highest activities for a first-row transition metal catalyst in water.[6–8] The proposed hydrogenation mechanism is depicted in red in **Scheme 2**. To obtain the electrochemical potential and pH requirements to generate the metal hydride intermediate, we measured the pK_a and reduction potential shown in blue in **Scheme 2**.

Scheme 1. Metal hydride generation through hydrogenation (gray) vs electrochemical methods (red).

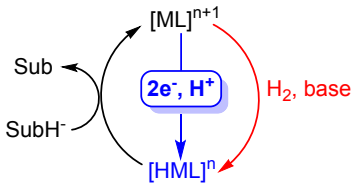

Scheme 2. Proposed electrocatalytic cycle for CO_2 reduction using $[Co(dmpe)_2(H)_2][BF_4]_2$ (**1**).

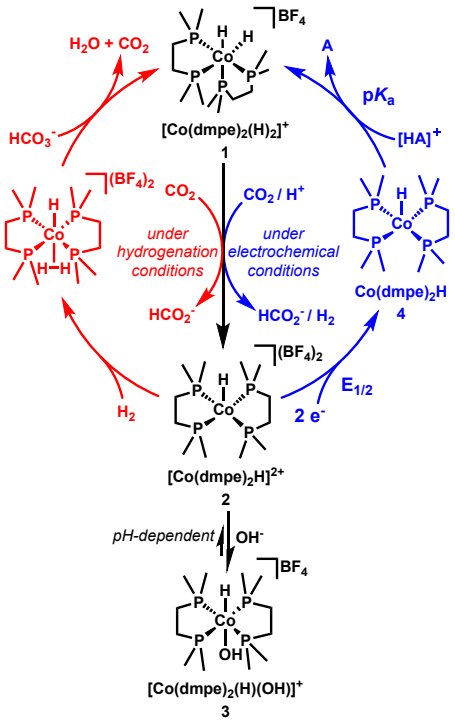

The synthesis and characterization of the dihydride $[Co(dmpe)_2(H)_2][BF_4]$ (**1**), $[Co(dmpe)_2H][BF_4]_2$ (**2**), $[Co(dmpe)_2(H)(OH)][BF_4]$ **(3),** and $Co(dmpe)_2H$ (**4**) were previously reported.[6,9] Our attempts to synthesize $[Co(dmpe)_2(H)_2][BF_4]$ (**1**) by the published method, reaction of $[Co(dmpe)_2][BF_4]_2$ (**2**) with KC_8 in acetonitrile under 1 atm H_2, resulted in the formation of an unidentified side product which we could not separate from **1**. Instead, we synthesized $[Co(dmpe)_2(H)_2][BF_4]$ (**1**) using $Co(C_5(CH_3)_5)_2$ as the reductant and then exposed to 1 atm of H_2 (see SI). $[Co(dmpe)_2(H)_2][BF_4]$ (**1**) was further characterized by low

[a] *Department of Chemistry, University of California, Irvine, Irvine, CA 92697, USA*
Electronic Supplementary Information (ESI) available: experimental details, NMR spectra, electrochemical data, electronic absorption spectra. See DOI: 10.1039/x0xx00000x

temperature $^{31}P\{^1H\}$, ^{31}P, and ^1H NMR spectroscopy (**Figures S1-S4**) and UV-Vis characterization of $[Co(dmpe)_2(H)_2]^+$ (**1**) and $[Co(dmpe)_2(OH)H][BF_4]$ (**3**) (**Figures S5-S6)**.

The pK_a of **1** was measured to determine the pH conditions necessary to generate the active catalyst from the reduced complex $Co(dmpe)_2H$ (**4**). When $[Co(dmpe)_2(H)_2]^+$ (**1**) is dissolved in pH 13.3, 13.2, and 13.1 phosphate buffer, it is partially deprotonated to form $Co(dmpe)_2H$ (**4**) (**Figure S7**). Based on the equilibrium product distribution between **1** and **4** measured at these different pH values, the pK_a of $[Co(dmpe)_2(H)_2]^+$ (**1**) is 12.9(5), providing the upper bound for the pH required to generate the hydride *in situ*.

Electrochemical characterization was conducted on solutions of $[Co(dmpe)_2(OH)H][BF_4]$ (**3**) below pH 12 to ensure that $Co(dmpe)_2H$ (**4**) would fully protonate to form $[Co(dmpe)_2(H)_2]^+$ (**1**) upon reduction. In water, $[Co(dmpe)_2(OH)H][BF_4]$ (**3**) is in equilibrium with $[Co(dmpe)_2H][BF_4]_2$ (**2**) (Scheme 1) due to hydroxide coordination.[6] However, at the pH conditions studied by cyclic voltammetry (7.9 and 9.9), only **3** is observed in solution by $^{31}P\{^1H\}$ NMR.

The reduction of $Co(dmpe)_2(OH)H]^+$ (**3**) at pH 9.9 in bicarbonate buffer under N_2 features two reduction events (**Figure 1**). An irreversible reduction at –0.96 V vs. SCE is attributed to the $Co^{3+/2+}$ reduction and a second event at –1.58 V is attributed to the $Co^{2+/+}$ reduction (**Figure 1,** red trace). This data is summarized in **Table 1**. The peak current increases linearly with the square root of scan rate for both reductions, indicating that the analyte is homogeneous and freely diffusing (**Figure S8**). The first reduction at -0.96 V is irreversible for scan rates between 50 mV/s to 1000 mV/s (**Figure S9**).

In bicarbonate buffer under N_2 (pH 9.9), we attribute the larger current associated with the $Co^{2+/+}$ reduction compared to the $Co^{3+/2+}$ reduction (**Figure S10**) to catalytic H_2 production, which was verified by controlled potential electrolysis (*vide infra*). The current increase is adjacent to background H_2 production at the electrode. At slow scan rates, no oxidation peak is observed for this reduction event (**Figure S11, top**). A return oxidation peak is observed at scan rates >100 mV/s. (**Figure S11, bottom**).

Under CO_2-saturated conditions, the bicarbonate solution acidifies to pH 7.9. The $Co^{3+/2+}$ reduction shifts anodically (–0.92 V vs. SCE) but remains irreversible (**Figure 1**). The onset potential for the $Co^{2+/+}$ reduction also shifts anodically by about 65 mV, and a modest increase in current is observed at –1.58 V vs. SCE (**Figure 1**). The oxidation peak at –1.48 V is not observed at faster scan rates, even at scan rates up to 1000 mV/s (**Figure S12**).

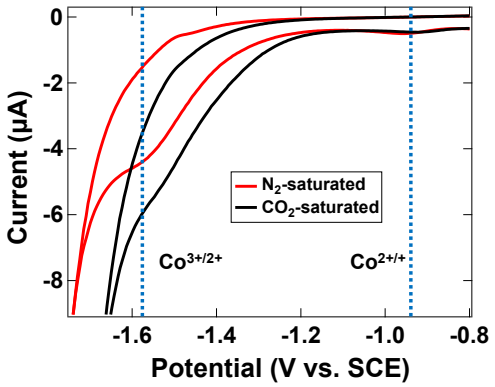

Figure 1. Cyclic voltammograms of 1 mM $[Co(dmpe)_2(OH)H]^+$ in 0.4 M bicarbonate buffer (pH 9.9, red trace) at 250 mV/s and after CO_2 addition (pH 7.9, black trace) using a glassy carbon disk working electrode. The reductions attributed to $Co^{3+/2+}$ and $Co^{2+/+}$ are labelled with blue dotted lines.

Another reduction event is only observed in bicarbonate buffer at pH 9.9, or in phosphate buffer after CO_2 is added to the solution, upon which the pH lowers to 7.9 and bicarbonate is producd *in situ*. This quasi-reversible reduction event at –0.62 V vs. SCE. This feature is not observed in phosphate buffer at pH 7.9 with no added CO_2 (**Figure S13**), suggesting that this feature may be due to bicarbonate interaction with the cobalt species, but no catalysis is observed at this event.

Controlled potential electrolysis (CPE) experiments were performed with **3** at –1.50 V vs. SCE using a 0.2 M sodium carbonate solution saturated with CO_2 to the appropriate pH value. Results from these experiments are summarized in **Table 2**. Formate was quantified by ^1H NMR and H_2 by gas chromatography. Under electrolytic conditions, the Faradaic yield for formate is optimized at pH 7.8. At other pH conditions, the Faradaic efficiency for H_2 is higher than that of formate. Electrolysis was also performed on blank samples containing only carbonate buffer acidified to the appropriate pH using CO_2 at –1.50 V vs. SCE. H_2 was observed under these conditions, but no formate was observed in solution for electrolyses without **3** present.

For this catalyst, using the applied potential at pH 8 (-1.5 V vs. SCE), we estimate the overpotential to be 800 mV (see SI). By comparison, two selective catalysts for CO_2 reduction to HCO_2^-,

Table 1. Electrochemical data for $[Co(dmpe)_2(OH)H]^+$ in bicarbonate buffered solutions at 250 mV/s.[a]

	Under N_2 (pH 9.9)		Under CO_2 (pH 7.9)	
	E_{pc} (V vs. SCE)	E_{pa} (V vs. SCE)	E_{pc} (V vs. SCE)	E_{pa} (V vs. SCE)
$Co^{3+/2+}$	-0.96	---	-0.92	---
$Co^{2+/+}$	-1.58	-1.48	-1.58	---

[a]Cyclic voltammograms were performed using 0.4 M bicarbonate buffer under N_2 (pH 9.9), or saturated CO_2 in 0.4 M bicarbonate buffer (pH 7.9) with the buffer acting as electrolyte. The reference electrode was a saturated calomel electrode (SCE); the working and counter electrodes were glassy carbon disk and rod respectively.

Table 2. Summary of CPE data with $[Co(dmpe)_2(OH)H]^+$ (**3**).[a]

	Charge passed (C)	Faradaic yield (% H_2)	Faradaic yield (% HCO_2^-)
pH 7.2	6.7 ± 0.5	52 ± 6	40 ± 7
pH 7.8	5.3 ± 0.8	47 ± 5	54 ± 4
pH 8.1	5.8 ± 0.5	57 ± 3	37 ± 2
pH 8.7	5.2 ± 0.7	62 ± 2	22 ± 5

[a]Experiments were conducted with 2 mM of analyte (0.01 mmol) using a glassy carbon rod working electrode, a carbon fabric counter electrode, and a SCE reference electrode in 0.2 M CO_2-saturated carbonate buffer. The solutions were electrolyzed at -1.50 V vs. SCE for 5 h over a mercury pool in the working electrode compartment.

Ir(POCOP) and $[Fe_4N(CO)]^-$ have overpotentials of 950 mV and 500 mV at pH 7 and pH 8 respectively (see SI for details).[10,11]

The energetic requirements for electrocatalytic reduction may exceed what is expected based on hydrogenation activity. For example, Waymouth and coworkers have translated the activity of reversible ruthenium hydrogenation catalysts to electrocatalytic alcohol oxidation, but observe a high overpotential. The overpotential is postulated to arise from the use of a very strong base.[24] Based on our prior work in acetonitrile, we expected catalysis to occur at low overpotentials because hydride transfer to CO_2 is nearly ergooneutral.[25] However, the pH values required to generate **1** limits the operational range of the catalyst.

To understand why pH-dependent product selectivity was observed, additional experimental and thermochemical analyses were performed.

Stoichiometric hydride transfer studies were conducted with $[Co(dmpe)_2(H)_2]^+$ (**1**) to compare the competitive reactivity with CO_2 or H^+ under 1 atmosphere of CO_2 under various pH conditions. Formate was quantified by ^1H NMR and H_2 by gas chromatography. The yields from these experiments using $[Co(dmpe)_2(H)_2]^+$ indicate that H_2 is the favored species under most conditions (**Table 3**). Formate reaches near-parity at pH 7.8.

The stoichiometric reactivity suggests that protonation of the cobalt hydride to form H_2 is a significant source of consumption of $[Co(dmpe)_2(H)_2]^+$ between pH 7 and pH 9. Consequently, we believe that the H_2 evolution observed during electrolysis likely arises from the catalyst itself, and not the electrode, which is further corroborated by bulk electrolysis experiments using a mercury pool working electrode. Mercury was chosen because the solvent window in water is shifted more negative for Hg than for glassy carbon, which means that H_2 production is less favorable for Hg compared to glassy carbon.[12] However, selectivity for formate did not improve with this electrode and a small amount of H_2 was still produced, indicating that the H_2 observed during electrolysis with $[Co(dmpe)_2(OH)(H)]^+$ in solution comes from the catalyst, not the glassy carbon electrode (**Table S1**).

The mixed product selectivity can be rationalized with the thermochemistry of hydride transfer to CO_2 and hydride transfer to H^+. This hydrogen evolution reaction (HER) typically proceeds through the protonation of metal hydride intermediates.[13] In order to rationalize the mixed product selectivity, we analyzed the free energies for the reaction of H^+ and CO_2 with $[Co(dmpe)_2(H)_2]^+$ (**1**) (blue center line, **Scheme 2**). The free energy for all reactions involving protonation of a metal hydride to form H_2 relies on the hydricity the former, proton activity (pH or pK_a) of the solution, and heterolytic cleavage energy of H_2 according to eq 1.[14]

$$\Delta G^{o}_{HER} = \Delta G^{o}_{H^-} + 1.364 * pK_a - \Delta G^{o}_{H_2}$$

The free energy for the CO_2 reduction reaction (CO2RR) via hydride transfer to form formate only relies on the relative hydricities of the metal hydride and formate (eq 2).[14]

$$\Delta G^{o}_{CO_2RR} = \Delta G^{o}_{H^-(MH)} - \Delta G^{o}_{H^-(HCO_2^-)}$$

In many cases, particularly in the well-studied group 10 class of bis(diphosphine) metal hydrides, the absence of a ligand coordination step concomitant with hydride transfer means that the hydricity value of a given metal hydride does not vary with pH.[15,16] As a result, there are conditions in which the reactivity of a metal hydride can reliably be predicted to be exergonic with CO_2 and endergonic with H^+, leading to product selectivity for the former.

In contrast, the reactivity of complexes that undergo ligand association after hydride transfer are do not remain invariant, especially under aqueous conditions.[17] As previously described by Wiedner and coworkers, the hydricity value of $[Co(dmpe)_2(H)_2]^+$ (**1**) is pH-dependent in water. The formation of the hydroxide bound species, $[Co(dmpe)_2(OH)H]^+$ (**3**) (eq 3) increases the *effective* hydricity of **1**, as the free energy includes formation of the Co-OH bond.[18,19] Increasing amounts of OH^- in solution at higher pH values therefore *increases* the hydricity of $[Co(dmpe)_2(H)_2]^+$ according to eq 3, where $\Delta G°_{H^-}$ is 14.0 kcal/mol as determined by a thermodynamic cycle (dashed blue line, Figure 2).[6]

(3) $[Co(dmpe)_2(H)_2] + OH^- \rightleftharpoons [Co(dmpe)_2(OH)H]^+ + H^-$

$\Delta G°_{H^-(eff)} = \Delta G°_{H^-} + 1.364*pOH$

Because the effective $\Delta G°_{H^-}$ of $[Co(dmpe)_2(H)_2]^+$ (**1**) is pH dependent (pOH = 14-pH), the free energy of H^- transfer to CO_2 is also pH dependent, while the free energy of HER remains the same value at all pH values. As a result, the free energy of hydrogen evolution $\Delta G°_{HER}$ is –1.1 kcal/mol at all pH values (black line, **Figure 2**).

While the free energy of the reaction of $[Co(dmpe)_2(H)_2]^+$ with CO_2 is more exergonic than H^+ above pH 7.4, stoichiometric and faradaic yields indicate that H_2 production is still the predominant reaction above pH 8. Data from cyclic voltammograms are also in

Table 3. Average yields from 3 trials of stoichiometric hydride transfer of $[Co(dmpe)_2(H)_2]^+$ (0.01 mmol) to either H^+ or CO_2.[a]

	% yield H_2	% yield HCO_2^-
pH 7.2	60 ± 9	33 ± 5
pH 7.8	47 ± 4	43 ± 7
pH 8.1	56 ± 6	47 ± 3
pH 8.7	66 ± 7	28 ± 4

[a]Reactions were conducted in 0.2 M carbonate solutions with CO_2 added to reach the appropriate pH.

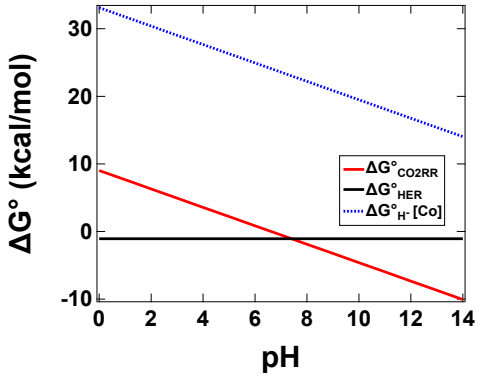

Figure 2. Thermodynamic relationships for CO_2 reduction, H_2 evolution, and $\Delta G°_{H^-(eff)}$ for $[Co(dmpe)_2(H)_2]^{2+}$. $\Delta G°_{CO2RR}$ and $\Delta G°_{HER}$ are calculated based on Eqs. 2 and 3 using $\Delta G°_{H^-(eff)}$ of $[Co(dmpe)_2(H)_2]^{2+}$.

agreement with this; despite acidifying the solution by adding CO_2 as a substrate, there is only a modest increase (< 40%) in the amount of current passed at –1.58V vs. SCE (**Figure 1**).

Although the free energy for hydride transfer from $[Co(dmpe)_2(H)_2]^+$ to CO_2 becomes more favorable at higher pH, the selectivity for formate vs H_2 is reduced. This discrepancy may arise from the different concentrations of bicarbonate and dissolved CO_2 at higher pH values. Prior work with aqueous CO_2 hydrogenation catalysts have demonstrated significantly higher turnover frequencies using 34 atm of a gaseous 1:1 H_2/CO_2 mixture than with bicarbonate alone in solution, suggesting CO_2 is more easily reduced than bicarbonate.[20,21] However, the effective concentration of CO_2 is only about 1/10th that of HCO_3^- at pH 7.8 and the concentration of CO_2 further decreases relative to HCO_3^- as the pH increases.[22,23] Thus, we believe that the lower concentration of CO_2 at higher pH values are an important determinant in aqueous selectivity.

A complicating factor in electrochemical reduction that does not exist in hydrogenation is the direct reduction of protons to hydrogen.[26] Despite the challenges in favoring CO_2 reduction versus H_2 evolution in aqueous solvents, selective homogenous CO_2 reduction catalysts have been reported. In an Ir(POCOP) system developed by Brookhart and coworkers, the current passed at E_{pc} (–1.3 V vs. SCE) under 1 atm CO_2 was 2.2 times greater than the current passed under 1 atm Ar at the same scan rate.[10] The Ir system, unlike the Co system described here, demonstrated selective CO_2 reduction to formate with optimal selectivity at –1.65 V vs. SCE at pH 6.95. Computational work done by Goddard and coworkers indicates that the observed selectivity likely originates from kinetically disfavoring H_2 formation, possibly from the presence of *tert*-butyl groups inhibiting the approach of a water cluster.[27] An iron carbonyl cluster, $[HFe4N(CO)_{12}]^-$ used by Berben and coworkers also demonstrates selective CO_2 reduction to formate. Like the Ir(POCOP) system, the free energy of H^+ and CO_2 reduction by the cluster is favorable. However, an Eyring analysis of the rate-determining hydride transfer step to CO_2 showed that the transition barrier was stabilized by almost 14 kcal/mol in H_2O compared to a 95:5 MeCN/H_2O solution, which indicates that selectivity in this system also arises from kinetic considerations.[28] Thus, success in selective aqueous CO_2 reduction electrocatalysts have relied on favoring the kinetic reactivity of CO_2. Catalyst designs that can kinetically inhibit the hydrogen evolution reaction may be particularly valuable for aqueous catalysts.[29]

There are no conflicts to declare. Corresponding Author: j.yang@uci.edu

Acknowledgements

The authors are grateful for support by the US Department of Energy Office of Basic Energy Sciences Award DE-SC0020275.

Notes and references

(1) Cheon, J.; Yang, J. Y.; Koper, M.; Ishitani, O. *Acc. Chem. Res.* **2022**, *55* (7), 931–932.
(2) Francke, R.; Schille, B.; Roemelt, M. *Chem. Rev.* **2018**, *118* (9), 4631–4701.
(3) Bai, S.-T.; Smet, G. D.; Liao, Y.; Sun, R.; Zhou, C.; Beller, M.; Maes, B. U. W.; Sels, B. F. *Chem. Soc. Rev.* **2021**, *50* (7), 4259–4298.
(4) Bi, J.; Hou, P.; Liu, F.-W.; Kang, P. *ChemSusChem* **2019**, *12* (10), 2195–2201.
(5) Wang, F.; Cannon, A. T.; Bhattacharya, M.; Baumgarten, R.; VanderLinden, R. T.; Saouma, C. T. *Chem. Commun.* **2020**, *56* (81), 12142–12145.
(6) Burgess, S. A.; Appel, A. M.; Linehan, J. C.; Wiedner, E. S. *Angew. Chem. Int. Ed.* **2017**, *56* (47), 15002–15005.
(7) Jeletic, M. S.; Mock, M. T.; Appel, A. M.; Linehan, J. C. A *J. Am. Chem. Soc.* **2013**, *135* (31), 11533–11536.
(8) Jeletic, M. S.; Helm, M. L.; Hulley, E. B.; Mock, M. T.; Appel, A. M.; Linehan, J. C. *ACS Catal.* **2014**, *4* (10), 3755–3762.
(9) Mock, M. T.; Potter, R. G.; O'Hagan, M. J.; Camaioni, D. M.; Dougherty, W. G.; Kassel, W. S.; DuBois, D. L. *Inorg. Chem.* **2011**, *50* (23), 11914–11928.
(10) Kang, P.; J. Meyer, T.; Brookhart, M. *Chem. Sci.* **2013**, *4* (9), 3497–3502.
(11) Taheri, A.; Thompson, E. J.; Fettinger, J. C.; Berben, L. A. *ACS Catal.* **2015**, *5* (12), 7140–7151.
(12) Bard, A., J.; Faulkner, L. R. *Electrochemical Methods: Fundamentals and Applications*, 2nd ed.; John Wiley & Sons, Inc., 2001.
(13) Ceballos, B. M.; Yang, J. Y. *Proc. Natl. Acad. Sci.* **2018**, *115* (50), 12686–12691.
(14) Wiedner, E. S.; Chambers, M. B.; Pitman, C. L.; Bullock, R. M.; Miller, A. J. M.; Appel, A. M. *Chem. Rev.* **2016**, *116* (15), 8655–8692.
(15) Tsay, C.; Livesay, B. N.; Ruelas, S.; Yang, J. Y. *J. Am. Chem. Soc.* **2015**, *137* (44), 14114–14121.
(16) Ceballos, B. M.; Tsay, C.; Yang, J. Y. *Chem. Commun.* **2017**, *53* (53), 7405–7408.
(17) Pitman, C. L.; Brereton, K. R.; Miller, A. J. M. *J. Am. Chem. Soc.* **2016**, *138* (7), 2252–2260.
(18) Mathis, C. L.; Geary, J.; Ardon, Y.; Reese, M. S.; Philliber, M. A.; VanderLinden, R. T.; Saouma, C. T. *J. Am. Chem. Soc.* **2019**.
(19) Brereton, K. R.; Jadrich, C. N.; Stratakes, B. M.; Miller, A. J. M. *Organometallics* **2019**, *38* (16), 3104–3110.
(20) Federsel, C.; Jackstell, R.; Boddien, A.; Laurenczy, G.; Beller, M. *ChemSusChem* **2010**, *3* (9), 1048–1050.
(21) Burgess, S. A.; Kendall, A. J.; Tyler, D. R.; Linehan, J. C.; Appel, A. M. *ACS Catal.* **2017**, *7* (4), 3089–3096.
(22) J. Connelly, S.; S. Wiedner, E.; M. Appel, A. *Dalton Trans.* **2015**, *44* (13), 5933–5938.
(23) Wiedner, E. S.; Linehan, J. C. *Chem. – Eur. J.* **2018**, *24* (64), 16964–16971.
(24) Waldie, K. M.; Flajslik, K. R.; McLoughlin, E.; Chidsey, C. E. D.; Waymouth, R. M. *J. Am. Chem. Soc.* **2017**, *139* (2), 738–748.
(25) Cunningham, D. W.; Barlow, J. M.; Velazquez, R. S.; Yang, J. Y. *Angew. Chem. Int. Ed.* **2020**, *59* (11), 4443–4447.
(26) Barlow, J. M.; Yang, J. Y. *ACS Cent. Sci.* **2019**, *5* (4), 580–588.
(27) Johnson, S. I.; Nielsen, R. J.; Goddard, W. A. *ACS Catal.* **2016**, *6* (10), 6362–6371.
(28) Taheri, A.; Carr, C. R.; Berben, L. A. *ACS Catal.* **2018**, *8* (7), 5787–5793.
(29) Barlow, J. M.; Ziller, J. W.; Yang, J. Y. *ACS Catal.* **2021**, *11* (13), 8155–8164.